

## **Supporting Information**

### **Efficient Oxidative Decomposition of Jet-Fuel *exo*- Tetrahydrodicyclopentadiene (JP-10) by Aluminum Nanoparticles in a Catalytic Microreactor: An Online Vacuum Ultraviolet Photoionization Study**

Souvick Biswas<sup>a</sup>, Dababrata Paul<sup>a</sup>, Nureshan Dias<sup>b</sup>, Wenchao Lu<sup>b</sup>, Musahid Ahmed<sup>b\*</sup>, Michelle L. Pantoya<sup>c\*</sup>, Ralf I. Kaiser<sup>a\*</sup>

<sup>a</sup> Department of Chemistry, University of Hawai'i at Manoa, Honolulu, Hawaii 96822, United States

<sup>b</sup> Chemical Sciences Division, Lawrence Berkeley National Laboratory, Berkeley, California 94720, United States

<sup>c</sup> Mechanical Engineering Department, Texas Tech University, Lubbock, Texas 79409, United States

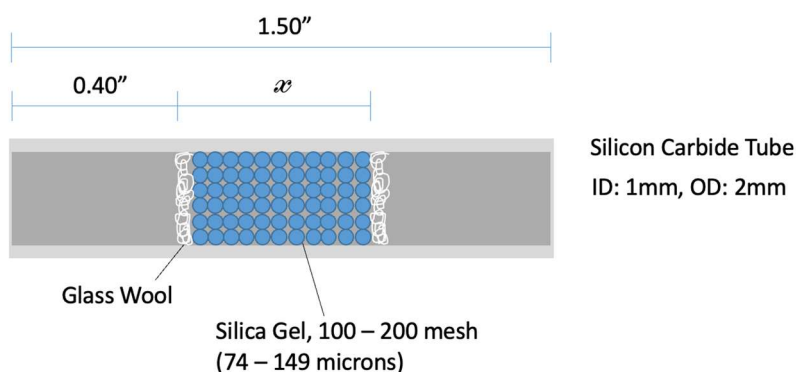
\* Corresponding author. E-mail: mahmed@lbl.gov

michelle.pantoya@ttu.edu

ralfk@hawaii.edu

## S1. Optimization of Catalyst Packing in SiC Microreactors

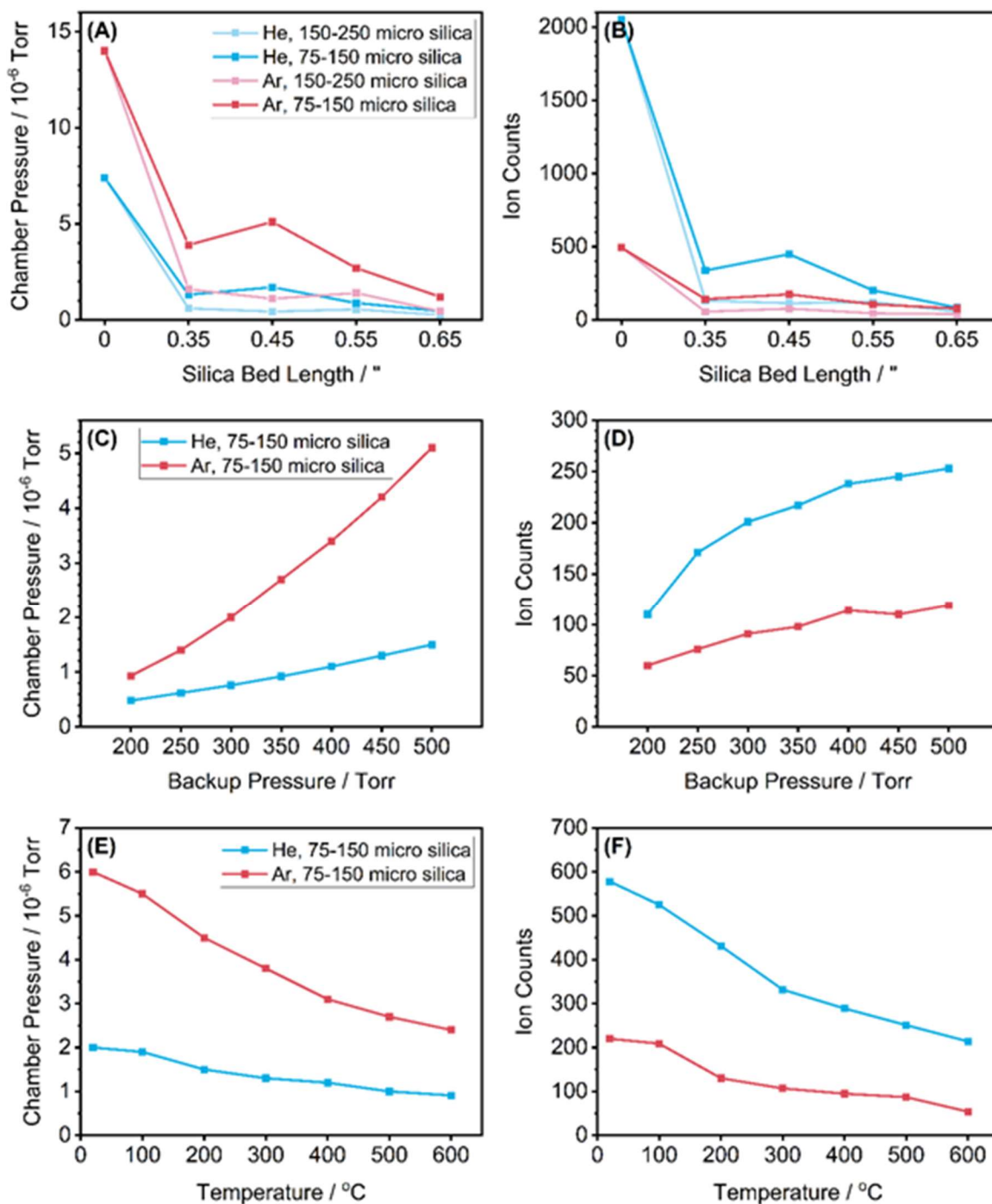
Before we loaded our SiC microreactor with catalytic aluminum nanoparticles, we conducted preliminary tests using silica. This approach was taken to assist us in evaluating the optimal packing methods. The factors that we needed to consider during this evaluation included the catalysis packing length, catalyst surface area, backup gas pressure, and reaction temperature. These factors can influence the residence time of the reactant gas in the reactor, which further leads to a significant change of the efficiency of the catalytic process. In a study conducted by Hemberger et al.<sup>1</sup> (*Nat. Commun.*, 2017, **8**, 15946), an annular packing method was employed, where the catalyst only adhered to the inner wall of the reactor. However, given the short length of our SiC reactor (~1.5 inches), we decided to adopt a compact packing method. In this method, the catalyst fills a short length ( $x$  in inches) inside the nozzle and is stopped on both sides using glass wool (**Scheme S1**). This method can help compensate for the short reactor length and increase the contact time between the gaseous reactants and the catalyst.



**Scheme S1:** The cross-section of a silica-packed SiC reactor

In our experimental setup, a bubbler containing pyridine at room temperature was seeded in 300 Torr of He or Ar. The gas mixture was then passed through the reactor packed with 100 – 200 mesh (74 – 149 microns) silica and expanded into a vacuum. We recorded the ion intensity and chamber pressures to better understand the influence of the catalyst bed length, surface area, and backup pressure (Figure S1). Initially, we tested with catalyst bed lengths ( $x$ ) ranging from 0.00 inches (empty reactor), 0.35, 0.45, 0.55, 0.65, to 0.75 inches. We observed that when the reactor was packed with a catalyst bed length of 0.35 inches from empty reactor, the signal intensity dropped significantly. In the case of He as the carrier gas, the intensity dropped to 1/6 whereas it dropped to 1/3 in the case of Ar. Interestingly, the intensity reached its maximum at approximately

0.45 inches. Beyond this, the ion intensity began to decrease as the bed length increased, albeit not sharply.



**Figure S1.** The changes of chamber pressure and ion counts by silica bed length, backup pressure, and reactor temperature.

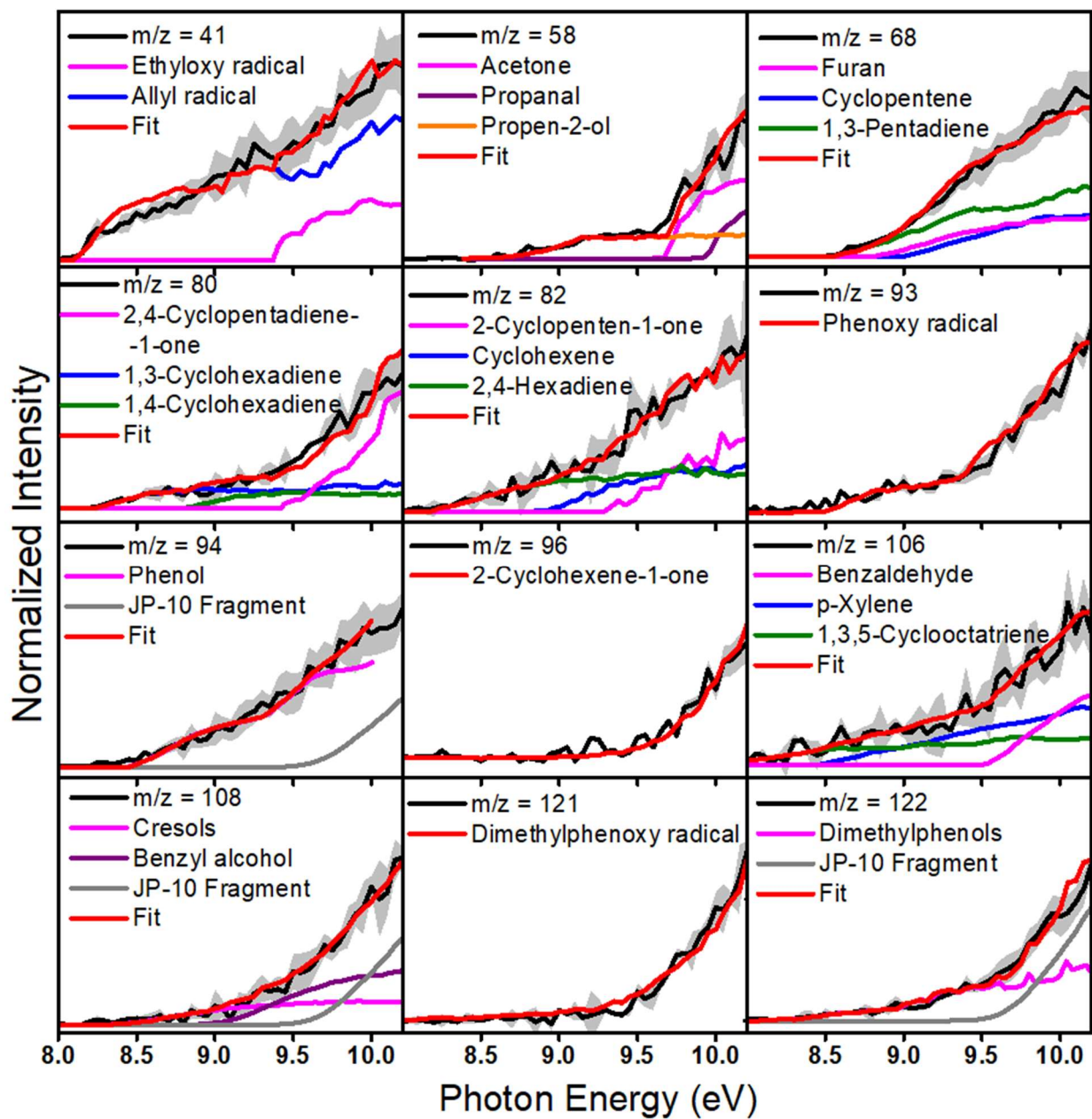
When the bed length reached above 0.55 inches, the signal took ~5 minutes to appear and approximately 30 minutes to reach equilibrium. We observed that the beam could possibly be choked at a bed length of 0.65 inches or higher. Both He and Ar carrier gases resulted in similar trends, but Ar exhibited poorer permeability through the packed silica and had a higher chamber pressure than He. As a result, the ion intensity of Ar was less than half of He under the same conditions.

We also compared these results with experiments using 60 – 100 mesh (149 – 250 microns, larger size) silica to investigate the influence of particle size (surface area). Although silica does not react with pyridine, its porous nature has resulted in a larger surface area for smaller particle size, which could absorb more molecules and thus influence the results. The results from both experiments showed a similar trend, and He performed better than Ar in both datasets. Larger particle sizes reduced the chamber pressure and ion intensity by half compared to smaller particles sizes (74 – 149 microns). Meanwhile, larger particles (149 – 250 microns) also had a lower overall surface area, which may reduce the efficiency of catalysis. Interestingly, with larger particle sizes, the signal maximum has shifted to a bed length of 0.55 inches from 0.45 inches in smaller particles size results, which suggests the use of smaller particle sizes for future experiments.

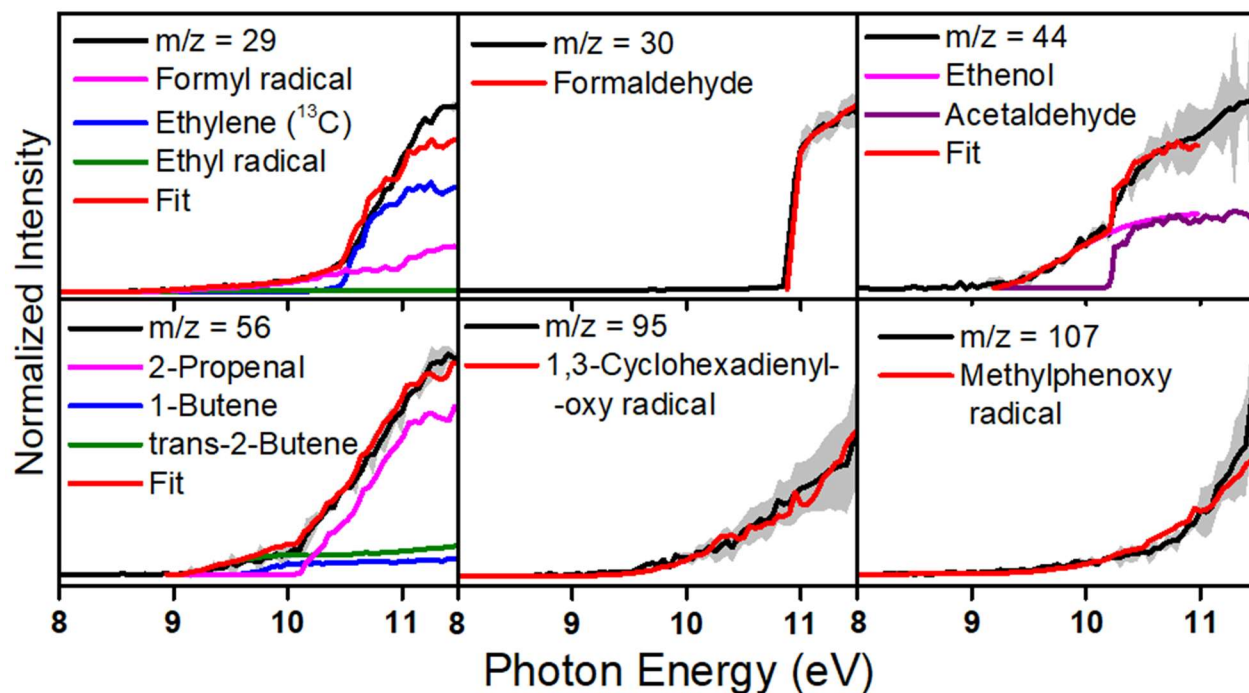
In addition, we studied the influence of different backup pressures ranging from 200 – 500 Torr, using a bed length of 0.55 inches. Our results indicated that the effect of pressure may not be significant. The intensity almost doubled when the pressure was increased from 200 to 300 Torr but did not change substantially when the pressure was increased from 300 to 500 Torr. Furthermore, from 300 to 500 Torr, He gas exhibited a less pronounced increase (1.25 times) in ion intensity compared to Ar gas (1.31 times). However, increasing the pressure also heightened the risk of silica being blown out. This suggests that the pressure should be maintained at 300 Torr for future experiments.

Finally, we investigated the influence of temperature, varying it from room temperature to 600°C. The packed hot nozzle functioned well up to 600°C (873 K). However, the ion intensity dropped as the temperature increased, possibly due to the expansion of particle size at high temperatures, which could potentially choke the molecular beam. At 600°C, the ion intensity dropped to 1/3 of that observed at room temperature. Though the ion intensity could be recovered when the temperature resumed, it required approximately 5 minutes to reach equilibrium.

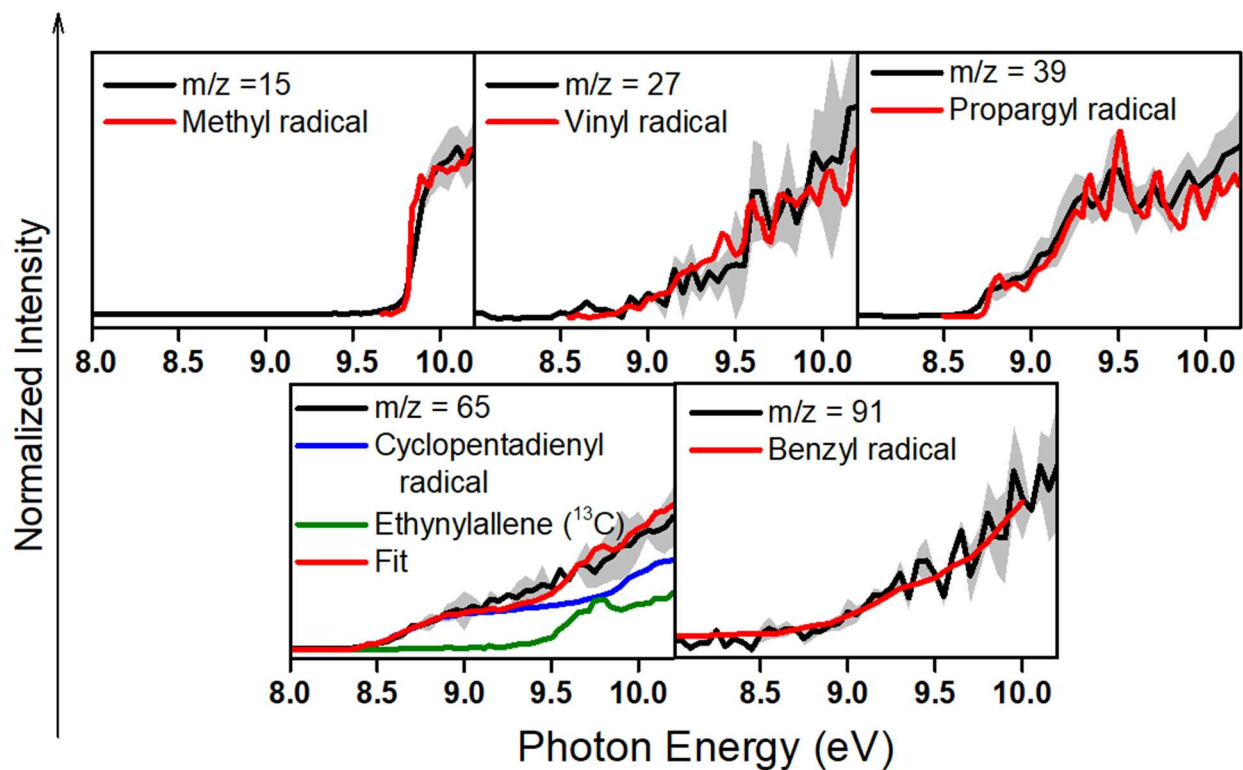
(A)



(B)

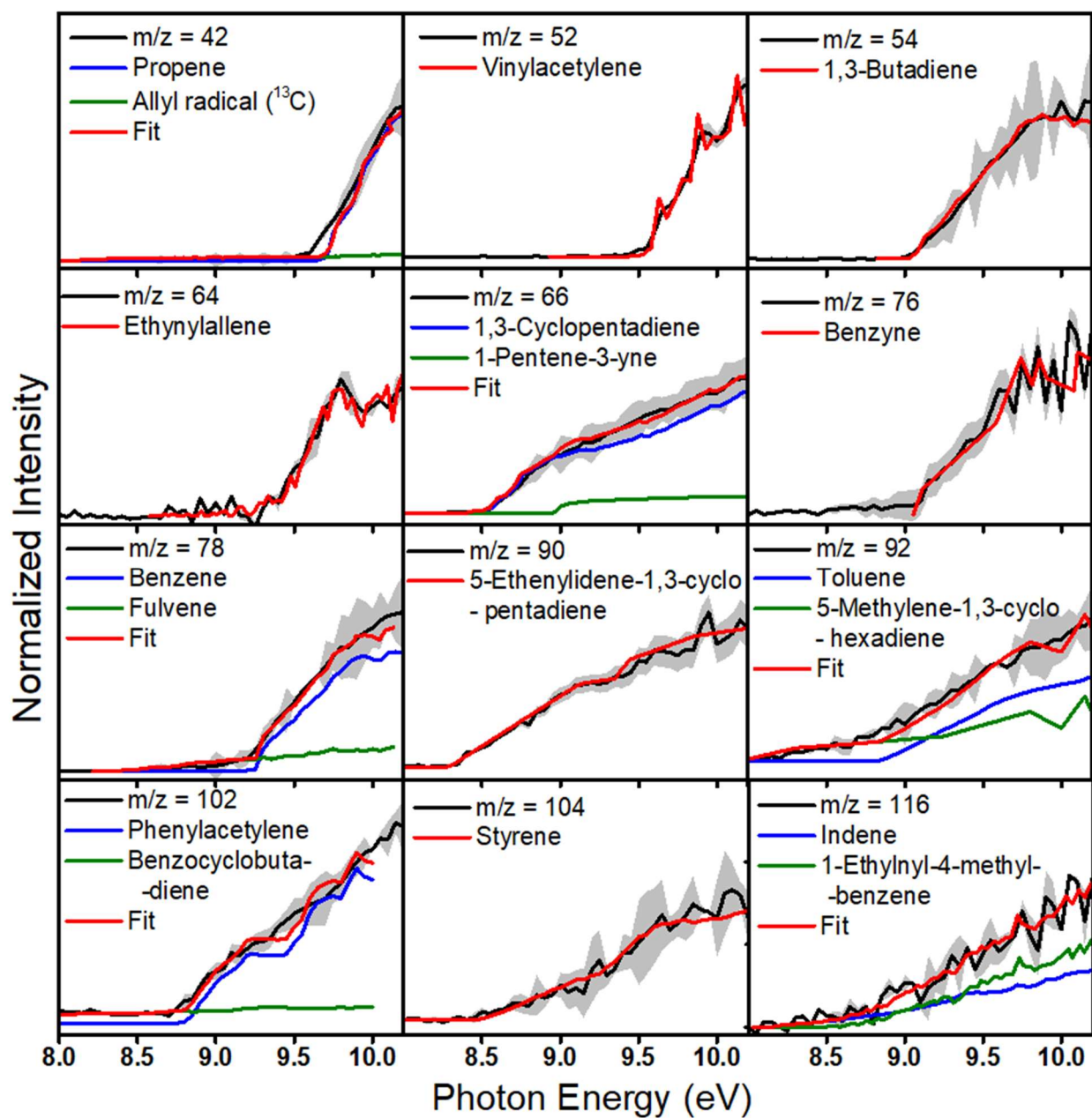


**Figure S2:** Experimental photoionization efficiency curves (PIE, black traces) in the range of (A) 8.0 - 10.2 eV and (B) 8.0 - 11.5 eV for the oxidized products (magenta, purple and orange reference traces) formed by the oxidation of JP-10 without any additive along with the experimental errors (gray shaded area). The errors originate from the measurement errors of the photocurrent by photodiode and a  $1-\sigma$  error of the PIE curves averaged over the individual scans. In case of multiple isomeric contributions, individual reference PIE curves are presented and the overall fitted curve is depicted by the red trace; the single component fits are also shown with red trace only. JP-10 fragment implies the photolysis fragment of JP-10 generated upon dissociative photoionization.



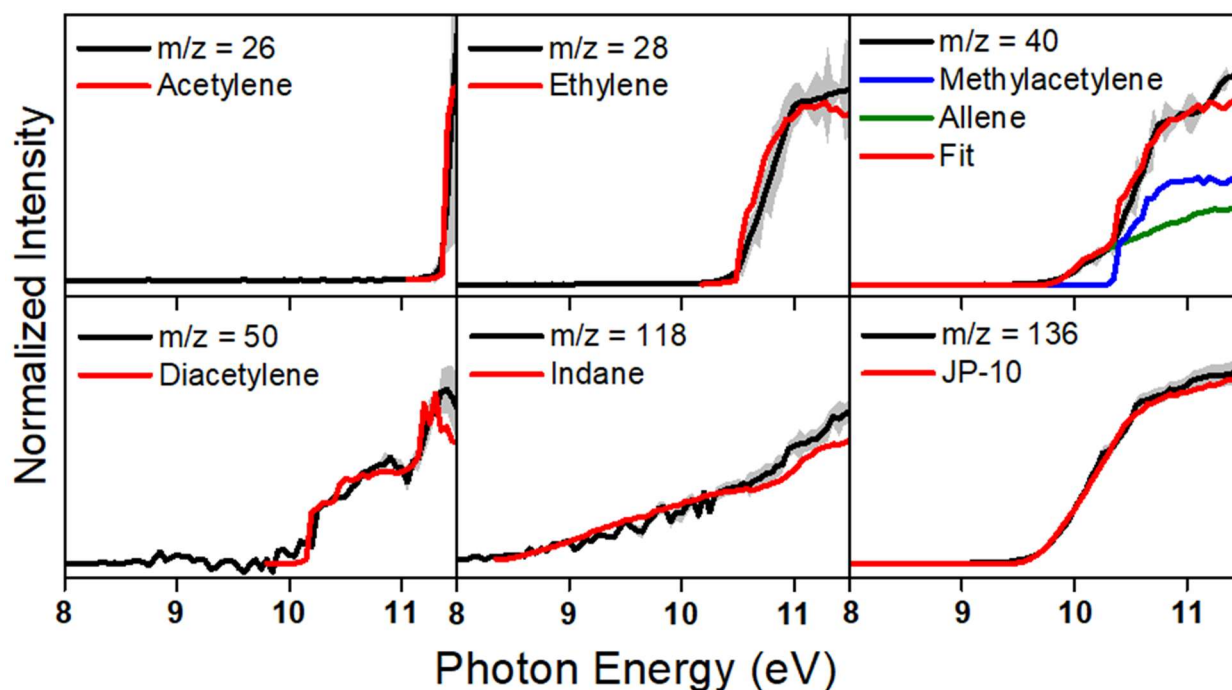
**Figure S3:** Experimental photoionization efficiency curves (PIE, black traces) for the hydrocarbon radical products formed during the oxidative decomposition of JP-10 without any additive along with the experimental errors (gray shaded area) originating from the measurement errors of the photocurrent by photodiode and a 1- $\sigma$  error of the PIE curves averaged over the individual scans. In case of multiple isomeric contributions, individual reference PIE curves are presented and the overall fitted curve is depicted by the red trace. JP-10 fragment implies the photolysis fragment of JP-10 generated upon dissociative photoionization.

(A)



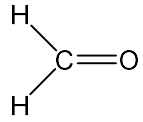
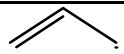
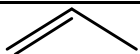
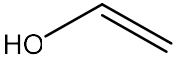
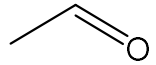
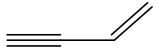
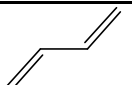


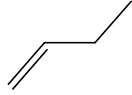
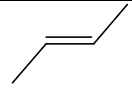
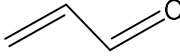
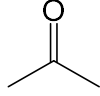
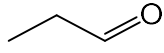
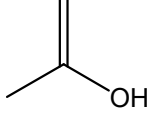
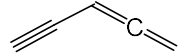
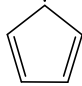
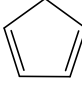
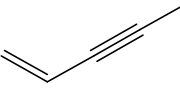

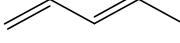
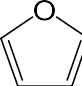


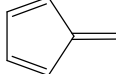
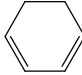
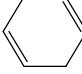
(B)

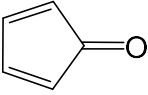
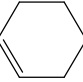
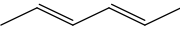
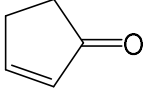
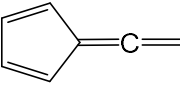
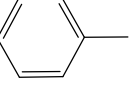
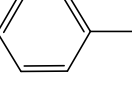
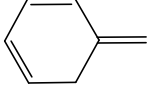
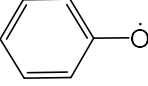
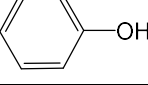
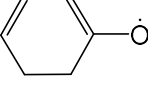
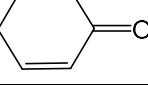
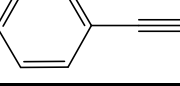
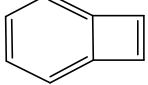
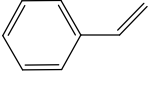
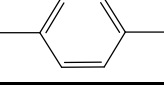


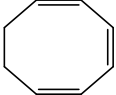
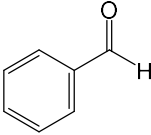
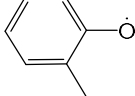
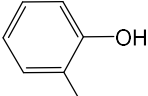
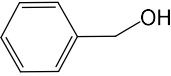
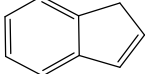
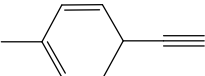
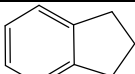
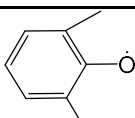
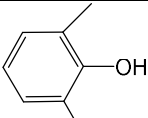
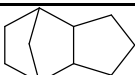
**Figure S4:** Experimental photoionization efficiency curves (PIE, black traces) in the range of (A) 8.0 - 10.2 eV and (B) 8.0 - 11.5 eV for the closed-shell hydrocarbon products (blue and green reference traces) generated during the oxidative decomposition of JP-10 without any additive along with the experimental errors (gray shaded area). The errors originate from the measurement errors of the photocurrent by photodiode and a 1- $\sigma$  error of the PIE curves averaged over the individual scans. In case of multiple isomeric contributions, individual reference PIE curves are presented and the overall fitted curve is depicted by the red trace; the single component fits are also shown with red trace only. JP-10 fragment implies the photolysis fragment of JP-10 generated upon dissociative photoionization.

**Table S1:** Details of the observed products and their appearances in the oxidation of JP-10 with and without AlNPs along with thermal decomposition of pure JP-10<sup>2</sup> and in presence of AlNP<sup>3</sup>.

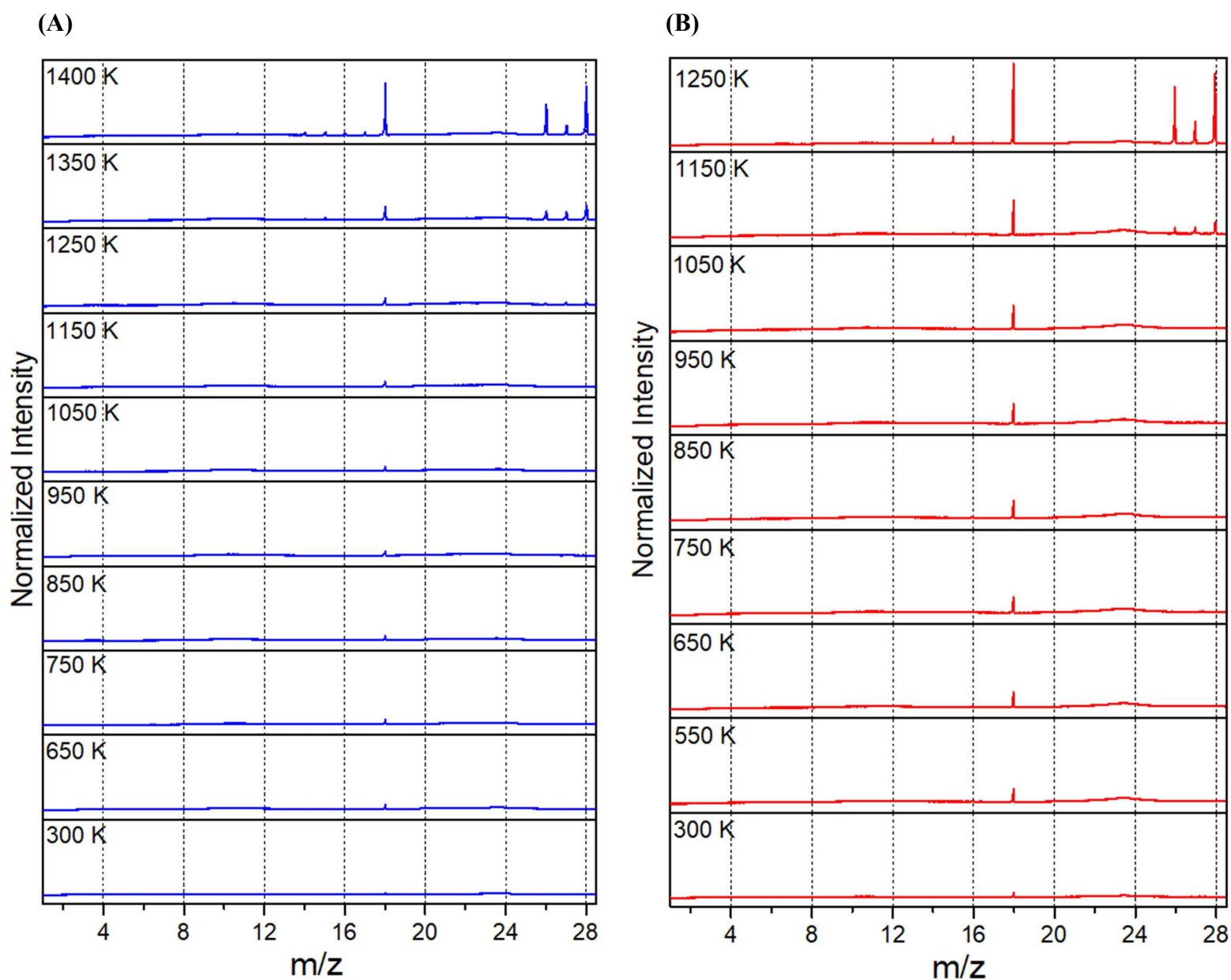
Mass	Molecular formula	Name	Structure	Reactant composition			
				JP-10 <sup>a</sup>	JP-10/ AlNP <sup>b</sup>	JP-10/ O <sub>2</sub> <sup>c</sup>	JP-10/ AlNP-O <sub>2</sub> <sup>c</sup>
2	H <sub>2</sub>	Hydrogen	H-H	+	+		
15	CH <sub>3</sub>	Methyl	CH <sub>3</sub> ·	+	+	+	+
16	CH <sub>4</sub>	Methane	CH <sub>4</sub>		+	+	+
18	H <sub>2</sub> O	Water	H <sub>2</sub> O		+	+	+
26	C <sub>2</sub> H <sub>2</sub>	Acetylene	≡≡≡	+	+	+	+
27	C <sub>2</sub> H <sub>3</sub>	Vinyl	≡≡·	+	+	+	+
28	C <sub>2</sub> H <sub>4</sub>	Ethylene	≡≡	+	+	+	+
29	C <sub>2</sub> H <sub>5</sub>	Ethyl	—·	+	+	+	+
	CHO	Formyl	H—C <sup>·</sup> =O		+	+	+
30	HCHO	Formaldehyde				+	+
39	C <sub>3</sub> H <sub>3</sub>	Propargyl	≡≡≡·	+	+	+	+
40	C <sub>3</sub> H <sub>4</sub>	Allene	≡C≡	+	+	+	+
		Methylacetylene	≡≡—	+	+	+	+
41	C <sub>3</sub> H <sub>5</sub>	Allyl		+	+	+	+
	C <sub>2</sub> HO	Ethynyloxy	HC≡C—O <sup>·</sup>		+		
42	C <sub>3</sub> H <sub>6</sub>	Propene		+	+	+	+
44	C <sub>2</sub> H <sub>3</sub> OH	Ethenol				+	+
	CH <sub>3</sub> CHO	Acetaldehyde				+	+
50	C <sub>4</sub> H <sub>2</sub>	Diacetylene	≡≡≡≡	+	+	+	+
52	C <sub>4</sub> H <sub>4</sub>	Vinylacetylene	≡≡— 	+	+	+	+
54	C <sub>4</sub> H <sub>6</sub>	1,3-Butadiene		+	+	+	+

56	C <sub>4</sub> H <sub>8</sub>	1-Butene		+	+	+	+
		2-Butene		+	+	+	+
	C <sub>3</sub> H <sub>4</sub> O	2-Propenal				+	+
58	C <sub>3</sub> H <sub>6</sub> O	Acetone			+	+	+
		Propanal			+	+	+
		Propen-2-ol				+	+
64	C <sub>5</sub> H <sub>4</sub>	Ethynylallene		+	+	+	+
65	C <sub>5</sub> H <sub>5</sub>	Cyclopentadienyl		+	+	+	+
66	C <sub>5</sub> H <sub>6</sub>	1,3-Cyclopentadiene		+	+	+	+
	C <sub>5</sub> H <sub>6</sub>	1-Penten-3-yne			+	+	+
68	C <sub>5</sub> H <sub>8</sub>	Cyclopentene		+	+	+	+
		1,3-Pentadiene		+	+	+	+
	C <sub>4</sub> H <sub>4</sub> O	Furan			+	+	+
76	C <sub>6</sub> H <sub>4</sub>	<i>o</i> -Benzyne				+	+
78	C <sub>6</sub> H <sub>6</sub>	Benzene		+	+	+	+
		Fulvene		+	+	+	+
80	C <sub>6</sub> H <sub>8</sub>	1,3-Cyclohexadiene		+	+	+	+
		1,4-Cyclohexadiene		+	+	+	+

	$C_5H_4O$	2,4-Cyclopentadiene-1-one			+	+	+
82	$C_6H_{10}$	Cyclohexene		+	+	+	+
	$C_6H_{10}$	2,4-Hexadiene				+	+
	$C_5H_6O$	2-Cyclopenten-1-one			+	+	+
90	$C_7H_6$	Fulvenallene		+	+	+	+
91	$C_7H_7$	Benzyl radical			+	+	+
92	$C_7H_8$	Toluene		+	+	+	+
		5-Methylene-1,3-cyclohexadiene		+	+	+	+
93	$C_6H_5O$	Phenoxy radical			+	+	+
94	$C_6H_6O$	Phenol			+	+	+
95	$C_6H_7O$	1,3-Cyclohexadienyloxy			+	+	+
96	$C_6H_8O$	2-Cyclohexene-1-one			+	+	+
102	$C_8H_6$	Phenylacetylene		+	+	+	+
		Benzocyclobutene		+	+	+	+
104	$C_8H_8$	Styrene		+	+	+	+
106	$C_8H_{10}$	p-xylene		+	+	+	+

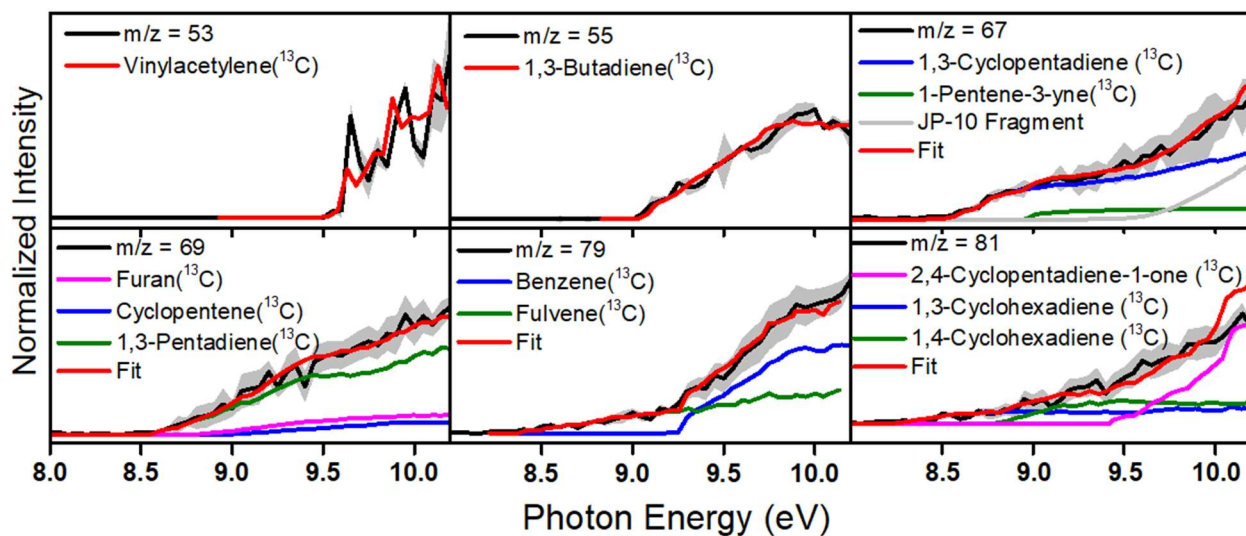
		1,3,5-Cyclooctatriene		+	+	+	+
	C <sub>7</sub> H <sub>6</sub> O	Benzaldehyde			+	+	+
107	C <sub>7</sub> H <sub>7</sub> O	Methylphenoxy radical			+	+	+
108	C <sub>7</sub> H <sub>8</sub> O	Cresols			+	+	+
		Benzyl alcohol			+	+	+
116	C <sub>9</sub> H <sub>8</sub>	Indene		+	+	+	+
		1-Ethynyl-4-methylbenzene			+	+	+
118	C <sub>9</sub> H <sub>10</sub>	Indane		+	+	+	+
121	C <sub>8</sub> H <sub>9</sub> O	Dimethylphenoxy radical			+	+	+
122	C <sub>8</sub> H <sub>10</sub> O	Dimethylphenol			+	+	+
136	C <sub>10</sub> H <sub>16</sub>	JP-10		+	+	+	+

*a: pyrolysis only<sup>2</sup>, b: pyrolysis in presence of AlNP<sup>3</sup>, c: this work (oxidation)*

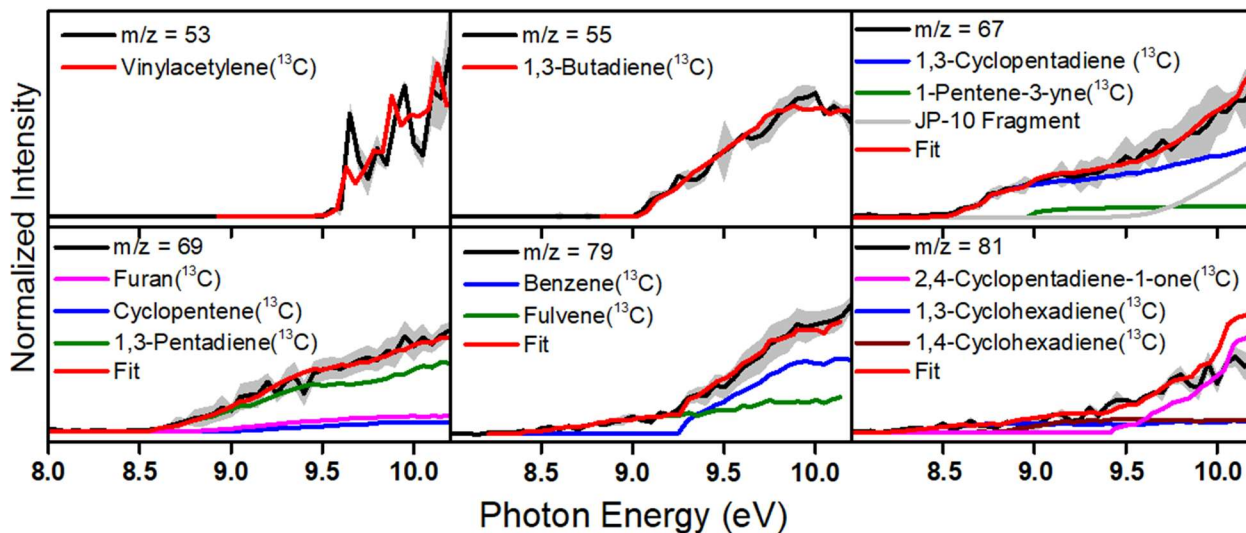


**Figure S5:** Segment of mass spectra of the products formed upon oxidation of JP-10 recorded at a photon energy of 15.4 eV in the 300-1,400 K temperature range, - (A) without and (B) with the aluminum nanoparticle (AlNP) packing inside the high-temperature chemical microreactor.

(A)



(B)



**Figure S6:** Experimental photoionization efficiency curves (PIE, black traces) for the mass peaks having contribution(s) from  $^{13}\text{C}$  only species in (A) presence and (B) absence of aluminum nanoparticles (AINPs). The experimental errors (gray shaded area) originate from the measurement errors of the photocurrent by photodiode and a  $1\text{-}\sigma$  error of the PIE curves averaged over the individual scans. In case of multiple isomeric contributions, individual reference PIE curves are presented and the overall fitted curve is depicted by the red trace; the single component fits are also shown with red trace only. JP-10 fragment implies the photolysis fragment of JP-10 generated upon dissociative photoionization.

## References:

- (1) Hemberger, P.; Custodis, V. B. F.; Bodi, A.; Gerber, T.; van Bokhoven, J. A. Understanding the Mechanism of Catalytic Fast Pyrolysis by Unveiling Reactive Intermediates in Heterogeneous Catalysis. *Nat. Commun* **2017**, *8*, 15946.
- (2) Zhao, L.; Yang, T.; Kaiser, R. I.; Troy, T. P.; Xu, B.; Ahmed, M.; Alarcon, J.; Belisario-Lara, D.; Mebel, A. M.; Zhang, Y.; et al. A Vacuum Ultraviolet Photoionization Study on High-Temperature Decomposition of JP-10 (Exo-Tetrahydrodicyclopentadiene). *Phys. Chem. Chem. Phys.* **2017**, *19*, 15780-15807.
- (3) Biswas, S.; Paul, D.; He, C.; Dias, N.; Ahmed, M.; Pantoya, M. L.; Kaiser, R. I. Counterintuitive Catalytic Reactivity of the Aluminum Oxide “Passivation” Shell of Aluminum Nanoparticles Facilitating the Thermal Decomposition of exo-Tetrahydrodicyclopentadiene (JP-10). *J. Phys. Chem. Lett.* **2023**, *14*, 9341-9350.